

Magnetoelastic Metamaterials for Energy Dissipation and Wave Filtering

Anna Guell Izard and Lorenzo Valdevit*

A novel magnetoelastic mechanical metamaterial consisting of a hyperelastic 2D lattice incorporating permanent magnets is presented and characterized. When properly designed and fabricated, the metamaterial possesses two stable equilibrium configurations (henceforth referred to as *hexagonal/hourglass* and *kagome*), both stretching dominated (and hence stiff). The two configurations have significantly different elastic properties and wave propagation characteristics, as shown numerically and experimentally. By switching between the two configurations via uniaxial loading cycles, the material displays hysteresis, thus dissipating substantial amounts of energy; in contrast with purely mechanical bistable structures (e.g., arches, hinged beams and buckled beams), the proposed magnetoelastic metamaterial does not require multiple unit cells in series or stiff boundary conditions to exhibit energy dissipation, thus enabling the implementation of compact stiff dampers. The presence of a bandgap in the kagome configuration (but not in the hexagonal/hourglass configuration) is attributed to an internal resonance mechanism and provides the foundation for the development of compact dynamic filters for mechanical signals.

Viscoelastic materials are routinely used to dissipate kinetic energy under impulsive (impact) and/or oscillatory (vibrations) loads. Unfortunately, dissipating energy requires high combinations of two material properties, Young's modulus and loss factor, which are generally in conflict in monolithic materials.^[1] This limitation can be overcome by designing architected materials incorporating negative stiffness elements within the unit cell. Negative stiffness, i.e., the reversal of the common sign in the relationship between force and displacement, by itself results in unstable mechanical behavior. Importantly, though, when negative stiffness elements, which possess a nonconvex strain energy landscape, are suitably combined with positive stiffness elements, a stable mechanical response at the architected material level can be achieved, whereas the internal degrees of

freedom in the topology can be exploited for energy dissipation, mechanical isolation, or other nonlinear phenomena.^[2]


Over the past few years, significant progress has been made on the analysis, fabrication, and characterization of cellular metamaterials with nonconvex strain energy landscape at the unit cell or subunit cell level. However, nearly all the negative stiffness elements used to date consist of arches,^[3–5] prebuckled beams,^[6] or rigid links connected by flexible hinges,^[7,8] all undergoing elastic snap-through. As the performance of all these elements is highly sensitive to boundary conditions, these designs present the major inconvenience that a stiff frame is required to constrain undesired deformations and secure a sharp negative stiffness region during snap-through. Furthermore, in most cases, a significant number of unit cells in series are required to obtain energy dissipation, potentially compromising compactness.^[9]

Magnetic elements are widely used in devices as energy harvesters, isolators, and dampers.^[10–12] Recently, a number of studies have appeared describing the incorporation of magnets and magnetic elements in devices and metamaterials, with the aim of altering their mechanical properties and/or wave propagation characteristics. For example, electromagnets were inserted in architected materials and structures to dramatically change their elastic properties,^[13] or to simultaneously achieve negative stiffness and negative Poisson ratio.^[14] The idea of using multistability (deriving from purely elastic or magnetoelastic effects) to tune wave propagation characteristics has also been recently explored by multiple researchers. The wave propagation characteristics in a bistable architected material consisting of multiple arches in series were analyzed, and the two configurations were shown to possess different bandgap widths, albeit only for wave propagation along one direction.^[15] A magnetoelastic bistable kagome lattice was also demonstrated, with the goal of exploiting large morphological changes enabled by the kagome topology combined with magnetoelastic interactions to design a multistable architected material with switchable dispersion characteristics.^[16] Despite all this work, to the best of our knowledge, the exploitation of magnetoelastic interactions to design bistable architected materials that exhibit both energy dissipation upon cyclic loading and tunable dispersion characteristics has never been demonstrated.

In this article, we explore the use of magnetic forces to design negative stiffness elements and create bistable architected

A. Guell Izard, Prof. L. Valdevit
Department of Mechanical and Aerospace Engineering
University of California, Irvine
Irvine, CA 92697, USA
E-mail: valdevit@uci.edu

Prof. L. Valdevit
Department of Materials Science and Engineering
University of California, Irvine
Irvine, CA 92697, USA

 The ORCID identification number(s) for the author(s) of this article can be found under <https://doi.org/10.1002/adem.201901019>.

DOI: 10.1002/adem.201901019

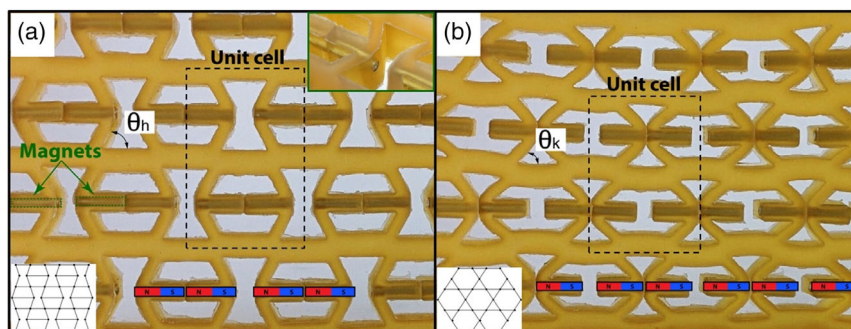


Figure 1. Magnetoelastic metamaterial. a) Image of the hexagonal/hourglass configuration of the lattice. The inset on the top shows a zoomed-in isometric view of the magnets. b) Image of the kagome configuration of the lattice. The dashed region represents the unit cell. Blue and red regions schematically represent the N and S poles of the inserted magnets.

materials which exhibit both energy dissipation and tunable wave filtering. We design and fabricate an elastomeric bistable architected material with embedded permanent magnets. By virtue of magnetoelastic interactions, the material has two equilibrium configurations, both stretching dominated under external uniaxial compressive loads. We can define the structure of the material as an alternation of hexagonal and hourglass units. In the hexagonal/hourglass configuration (**Figure 1a**), the magnetic force provides stiffness to the horizontal bars, thus limiting the horizontal deformation of the hexagonal cells. Upon uniaxial compression of the structure, the magnets will eventually separate and snap to the kagome configuration (**Figure 1b**), in which the hourglass unit transforms into two triangular cells, which are stabilized and stiffened by the presence of the magnets.

We analyze the quasistatic and dynamic response of the metamaterial. We first characterize the Young's and shear moduli of the material in the hexagonal/hourglass and kagome configurations, and, subsequently, we study the behavior of a single unit cell under a quasistatic loading/unloading cycle, demonstrating energy dissipation. Finally, we subject the metamaterial to mechanical waves impinging at different frequencies and demonstrate that only one configuration possesses a bandgap, thus enabling tunable mechanical filtering. All experimental results are used to validate finite element models.

Sample fabrication. Magnetoelastic architected materials are fabricated by casting urethane rubber in a 3D-printed mold. Permanent magnets are suspended in the mold by levitation prior to casting. The magnetoelastic architected materials are easily removed from the mold after curing. Details are provided in the Experimental Section and Figure S1, Supporting Information.

Effective elastic moduli. We fabricate 3 two-layer samples (1×2.5 unit cells; Figure S3 and S4, Supporting Information) and characterize the effective elastic properties of the metamaterial in the hexagonal/hourglass and kagome configuration. The effective moduli are also extracted by finite element analysis, whereby the materials are modeled as a two-coefficient Mooney–Rivlin hyperelastic solid (Figure S2a, Supporting Information). The results are shown in **Figure 2a,b**, with moduli normalized by the elastic constants of the parent elastomeric material, $E_s = 0.6$ MPa and $G_s = E_s/3 = 0.2$ MPa. Both the Young's and the shear moduli change significantly upon configurational change; in the hexagonal/hourglass configuration (**Figure 1a**),

the relative Young's modulus is ≈ 0.25 and the relative shear modulus is ≈ 0.12 ; when the architected material is switched to the kagome configuration, the Young's modulus decreases by a factor of ≈ 2 , whereas the shear modulus increases by a similar amount. Experimental and numerical results are in good agreement, with the numerical analysis consistently overpredicting the results by 4–11%. The change in moduli upon configurational change is attributed to the change in angle between the horizontal and the diagonal truss elements (**Figure 1**). Mechanics of materials considerations predict $\bar{E}_h/\bar{E}_k \approx \sin^2 \theta_h/\sin^2 \theta_k$ and $\bar{G}_h/\bar{G}_k \approx \cos^2 \theta_h/\cos^2 \theta_k$, where the subscripts h and k refer to the hexagonal/hourglass and kagome configurations, respectively (Supporting Information). For our fabricated samples, $\theta_h = 60^\circ$ and $\theta_k = 40^\circ$, hence $\bar{E}_h/\bar{E}_k \approx 1.85$ and $\bar{G}_h/\bar{G}_k \approx 0.43$, in good agreement with experimental measurements.

Energy dissipation under quasistatic cyclic loading. To characterize the mechanical behavior of the architected material under quasistatic cyclic loading, we fabricate and test a 0.5×3.5 unit cell sample. The result of the cyclic test is shown in **Figure 2d** (blue). The same experiment is modeled numerically using the finite element method. An implicit dynamic solver is used, to avoid convergence issues related to the rapid snap-through of magnets and ensure unconditional stability and rapid convergence.^[17] As before, the urethane rubber is simulated using a two-coefficient Mooney–Rivlin hyperelastic solid. Magnet–magnet interaction is modeled with connector elements with the same force–distance profile as our magnets (**Figure S2b**, Supporting Information) and with hard contact conditions in place to capture snapping. A schematic of the finite element simulation and contours of the von Mises stresses in one beam of the structure at various stages of loading and unloading are shown in **Figure 2c**. The resulting force–displacement curve is shown in **Figure 2d** (red). Note that the magnetoelastic metamaterial clearly exhibits substantial hysteresis upon cyclic loading, captured by both experiments and numerical analyses. In the experiment, the lattice snapped from the hexagonal/hourglass to the kagome configuration at a compressive displacement of 3.8 mm; the jagged snap is due to the fact that not all the magnets snap at the same time. Snap-back to the hexagonal/hourglass configuration upon unloading occurs at a compressive displacement of 0.6 mm and is again a jagged transition. This jagged transition

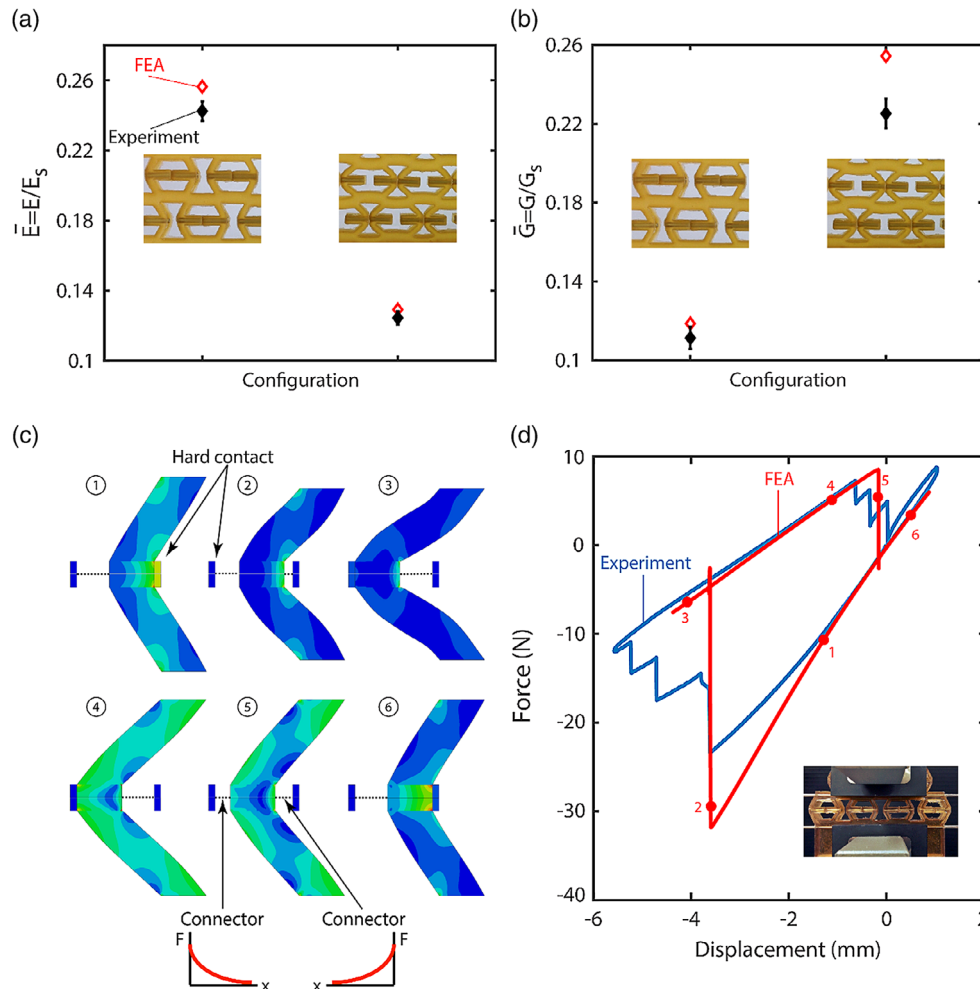


Figure 2. a) Normalized Young's modulus of the magnetoelastic metamaterial, in the hexagonal/hourglass and kagome configurations. Black (solid) symbols denote experimental results with standard deviation, red (open) symbols denote numerical predictions obtained with finite elements analysis (FEA). b) Normalized shear modulus of the magnetoelastic metamaterial, in the hexagonal/hourglass and kagome configurations. Black (solid) symbols denote experimental results with standard deviation, red (open) symbols denote numerical predictions. c) Sequence of deformation of two struts during axial cyclic loading in the vertical direction, predicted by finite element analysis. The solid rectangular regions represent the magnets. The beam is originally snapped in the hexagonal/hourglass configuration (1). At a critical compressive displacement, the right magnets detach (2) and the beams snap into the kagome configuration (3). Upon unloading (4), the magnets detach from the kagome configuration (5) and snap back into the hexagonal/hourglass configuration (6). d) Force–displacement relation for 0.5×3.5 unit cell sample under a full uniaxial loading cycle in the vertical direction. Notice the large hysteresis loop, indicating extensive energy dissipation. In blue, experimental results, in red, numerical prediction by finite element analysis, with the positions of points 1–6 from (c) marked.

has been shown to be consistent over multiple cycles on the same sample, but it is not identical among different samples (Figure S7, Supporting Information), demonstrating that the jagged transition is due to manufacturing imperfections (in particular, misalignments between magnets within each sample) and subtle sample/grips misalignment during mechanical testing. Overall, the finite element analysis shows good agreement with the experiment, in terms of qualitative shape of the curve, area under the hysteresis curve (i.e., energy dissipation), loads and displacements at the snap-through points, and sample stiffness. The only disagreement between modeling and experiment is on the sample stiffness upon loading, at compressive displacement larger than 1.5 mm. This discrepancy is largely attributed to instabilities during the test and the possible presence of

out-of-plane displacements in the experiment, which cannot be captured in the 2D numerical model. It is important to emphasize that the very significant loss coefficient exhibited by our magnetoelastic architected material cannot be attributed to the intrinsic damping of the elastomeric constituent material, as in the numerical analyses the elastomeric material is modeled as a lossless hyperelastic solid. Thus, the excellent agreement in the size of the hysteresis loop between model and experiment reveals that the intrinsic damping coefficient of the elastomer (estimated to be ≈ 0.1) has an insignificant effect on the overall energy dissipation in the magnetoelastic metamaterial. In other words, the energy dissipation mechanism exhibited by these materials is purely a structural phenomenon. The choice of an elastomeric material as our constituent solid is not motivated

by its viscoelastic properties but rather by its ability to experience very large elastic strains. The dissipated energy is released mainly through heat. The snap-through of the magnets is a rapid transition from a state with a higher potential energy to a state with a lower potential energy. During this transition, higher vibrational modes are activated, and the material quickly damps the energy, releasing heat. In our system, a portion of the energy is also released during the impact of the magnets.

It is worth mentioning that some mechanical negative stiffness metamaterials can be designed to be monostable and still dissipate energy.^[3] Here, we have limited our attention to bistable designs, as bistability enables wave filtering applications. In any case, our simulations indicate that monostable magnetoelastic metamaterials exhibit little-to-no hysteresis under cyclic loading.

An additional important feature of the proposed magnetoelastic metamaterial is that hysteretic behavior under cyclic loading (and hence energy dissipation) is present even from a single unit cell. Although purely mechanical concepts with single unit cell energy dissipation have been demonstrated,^[5,18] these concepts are geometrically complicated, challenging to fabricate and strongly affected by manufacturing imperfections and mechanical boundary conditions. In contrast, simpler bistable mechanical designs consisting of buckled beams or arches require multiple unit cells in series to display hysteretic behavior.^[9,18] Combined with the fact that the proposed design does not require a bulky external frame to constrain lateral displacements, this feature makes the proposed magnetoelastic design an ideal candidate for the fabrication of compact devices for energy dissipation.

To properly quantify the advantages of the proposed design relative to chains of bistable arches in series, we perform a parametric study of both concepts using nonlinear finite element analysis and extract comparisons for the relevant figures of merit (see Experimental Section and Supporting Information for more details). For both designs, we calculate the loss coefficient, defined as the quotient between the dissipated energy and the applied

energy, $\psi = U_{\text{diss}} / (0.5 \cdot F^{\text{max}} \cdot \gamma^{\text{max}})$, the normalized effective Young's modulus, E/E_s , and the maximum strain that the constituent material undergoes in a full cycle. It is worth mentioning that we are comparing the loss coefficient for an infinite chain of arches with the loss coefficient for a unit cell of the magnetoelastic material. In other words, we are comparing the upper bound of energy dissipation for the chain of arches with the lower bound of energy dissipation for the magnetoelastic material. The maximum energy that a chain of arches can dissipate is the area under the stress-strain curve of a single unit cell when the structure is tested under load control.^[2,9] In **Figure 3a**, we map the normalized Young's modulus versus the loss coefficient for both designs. A few important conclusions can be extracted: 1) the maximum loss coefficient that can be reached with both designs is similar and is around 3; 2) higher values of the normalized Young's modulus can be achieved with the magnetoelastic design; 3) higher values of the damping figure of merit, i.e., the product of the Young's modulus and the loss coefficient, can be obtained with the magnetoelastic design. In **Figure 3b**, we plot the damping figure of merit versus the maximum strain that the constituent material undergoes in a full cycle. Two key conclusions emerge: 1) the magnetoelastic material has a smaller range of maximum strain (8–70%) than the chain of arches (0.05–50%), thus limiting the magnetoelastic designs to constituent materials that can sustain strains in excess of 8% without plastic deformation or fracture, and 2) for any maximum strain in the range of 8–70%, the magnetoelastic material has up to an order of magnitude higher figure of merit than the chain of arches.

These differences between the two designs are attributed to the steep force-displacement response of the magnets: this behavior provides a higher negative stiffness than a snapping arch, resulting in a higher relative Young's modulus. For hysteresis to occur in a structure consisting of negative and positive stiffness springs in series, the positive stiffness spring must be more compliant than the negative stiffness spring.^[5,9] Our

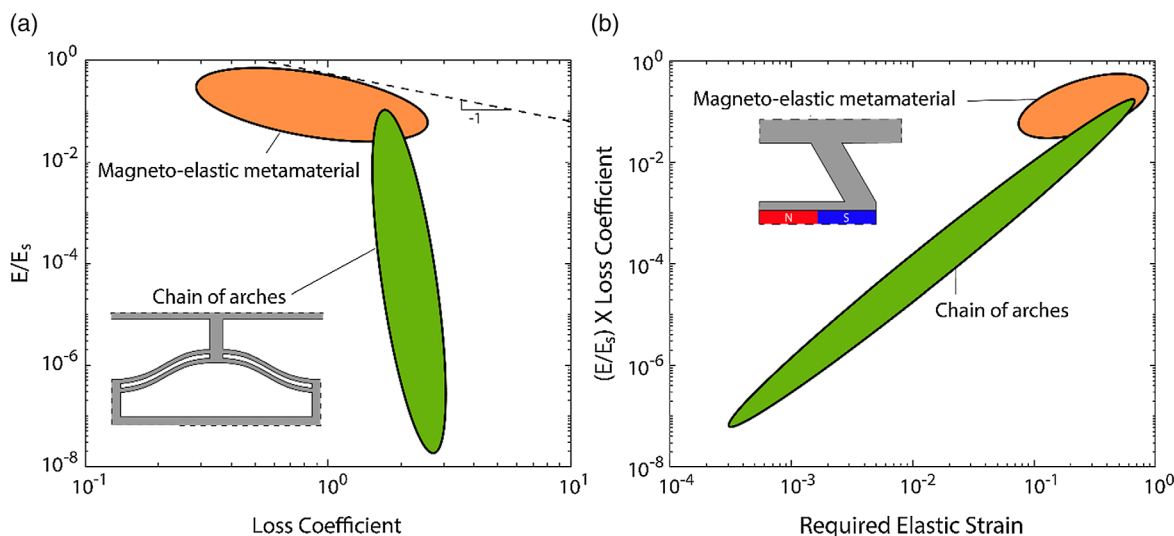


Figure 3. a) Normalized Young's modulus versus loss coefficient for the proposed magnetoelastic material, compared with an infinite chain of arches. b) Figure of merit (i.e., the product of the normalized Young's modulus and the loss coefficient) versus the required elastic strain (maximum strain that the constituent material undergoes) for the magnetoelastic metamaterial and the infinite chain of arches. All values have been obtained with nonlinear finite element analysis, as discussed in the text.

beam/magnet system can be understood as a simplified version of a spring (the constant of the spring is the stiffness of the beam) in series with a negative stiffness element; thus, the steep force–displacement relation in magnets allows our metamaterial to exhibit hysteresis even in a stretching dominated configuration, offering combinations of stiffness and loss coefficient that cannot be achieved with mechanical snap-through elements.

Wave propagation characteristics. The wave propagation characteristics of periodic structures are highly dependent on the topology of the unit cell and its stiffness, suggesting that the proposed bistable structure could be used as a mechanical filter. Plane wave propagation in periodic structures is analyzed through the application of the Bloch theorem, which allows us to calculate the eigenfrequencies of a periodic structure by analyzing a single unit cell subject to a specific set of periodic boundary conditions^[19,20] (see Experimental Section and Supporting Information for details). The eigenmodes for the different wave vectors and for both configurations, with normalized frequencies from 0 to 2.3, are shown in **Figure 4**. The frequencies are normalized by $f_s = (1/2\pi)\sqrt{E_s t^3 W / (L^3 (0.5m + tWL\rho_s))}$, where E_s is the Young's modulus of the constituent material, t is the thickness of the truss members, W is the depth of the sample, L is the length of one truss member, m is the mass of one magnet, and ρ_s is the density of the constituent material. In our case, $f_s = 154.9$ Hz. For this analysis, we have assumed that the connection between the magnets is strong enough that it can be considered a monolithic union, and the nearby magnets are sufficiently far away that they exert no force and contribute no stiffness. To verify the validity of the monolithic union approximation, we calculate the resonant frequency of the magnet-to-magnet connection, approximating it as a two-mass system linked with a linear spring. With a spring constant $k = 23.1$ N mm^{−1} (the stiffness of the connection) and a mass of the magnets $m = 0.75$ g, the resonant frequency of the connection is $f = \sqrt{2k/m}/2\pi = 1250$ Hz, which is three times higher than the maximum frequency we analyzed. Hence, under our experimental conditions, the magnet–magnet system behaves as a monolithic union even under dynamic conditions. We experimentally characterize wave propagation along the e_2 direction in both configurations (Figure 4). We manufacture a sample of 4×4 unit cells and suspend it with nylon wires. The setup of the experiment is shown in Figure 4c. The sample is excited at one end with an electrodynamic shaker, driven by a MATLAB script. The acceleration is measured at both ends of the sample, and the data are collected with MATLAB using a data acquisition system. For each specific frequency in the range of 50–350 Hz (with a step of 2 Hz), a sine wave is generated and maintained for 2 s. The transmittance is calculated as $T = 20 \log(A_f/A_i)$, where A_i is the amplitude of the acceleration at the end where the shaker is connected, and A_f is the amplitude of the acceleration at the other end. This experiment is repeated for both hexagonal/hourglass and kagome configurations. The results of the wave propagation analysis for both configurations are shown in Figure 4a,b. Notice that only the kagome configuration presents a bandgap, between the normalized frequencies of 1.5 and 1.8. The key implication is that any wave, with a frequency in that range will not be transmitted through the structure in the kagome configuration. Note that because the quarter unit cell does not have rotational symmetry (the unit cell has rectangular symmetry), the dispersion curves on the regions GX and

XM are different than the curves on GY and YM, respectively. The transmittances on the e_2 direction of a 4×4 unit cell are shown in Figure 4a,b, side by side with a theoretical bandgap map. A peak of isolation can be observed in the kagome configuration between 210 and 260 Hz. The bandgap is theoretically located between the normalized frequencies 1.6 and 2, approximately equivalent to 250 and 300 Hz in our case. Although the qualitative behavior is perfectly captured by the model, a discrepancy in the location of the bandgap exists. This discrepancy is primarily attributed to the substantial mass of the accelerometers, which is not properly modeled in the finite elements calculations, as well as to the intrinsic damping of the base material, the magnet–elastomer interfaces, and other manufacturing defects. The peak observed in the hexagonal/hourglass configuration at 330 Hz can be attributed to a directional bandgap on the GY region that theoretically is located at 380 Hz, at normalized frequency of 2.45 Hz (Figure S15, Supporting Information).

To elucidate the mechanism responsible for opening of the bandgap in the kagome configuration, we calculate the eigenfrequencies of the structure by finite element analysis and find a resonant frequency of the “horizontal magnet beam” at ≈ 280 Hz (the mode shape is shown in the inset in Figure 4b). As this frequency is close to the observed gaps, we conclude that the bandgap of the kagome configuration can be attributed to the local resonance of the “magnet beams.”^[21] In the hexagonal/hourglass configuration, this resonant mechanism is not present, as the magnets are well enclosed by the hexagonal units.

We have created a bistable cellular material encompassing permanent magnets. This structure is stretching dominated in both configurations under external uniaxial loads, yet the two configurations have significantly different elastic moduli. This magnetoelastic metamaterial offers impressive amounts of energy dissipation under loading and unloading cycles, amounts that are well captured by finite element analyses. In addition, the topological changes alter wave propagation characteristics, introducing a bandgap in only one (the kagome) configuration. This bandgap is clearly captured in the experiments. The use of magnets to implement negative stiffness components (as opposed to using traditional negative stiffness elements, e.g., buckled beams and arches) has allowed us to create a bistable metamaterial which does not require a stiff frame to constrain the mechanical elements undergoing snap-through. Another key advantage of magnetoelastic metamaterials is their ability to dissipate large fractions of input energy in a single unit cell system, a desirable feature enabled by the steep force–displacement relationship typical of magnets. This feature is in stark contrast with the behavior of periodic architected materials with purely mechanical negative stiffness implementations: in these systems, multiple unit cells in series (≈ 10 – 100 , depending on the topology and geometry of the system) are required in order for the architected material to display hysteretic behavior under cyclic loadings.^[9] The proposed magnetoelastic metamaterial can find important applications in bistable switchable mechanical wave filters and compact devices for energy dissipation.

Experimental Section

Materials: The constitutive material for all samples was urethane shore 20A rubber (Smooth-On, Inc., VytaFlex series). The depth of all samples

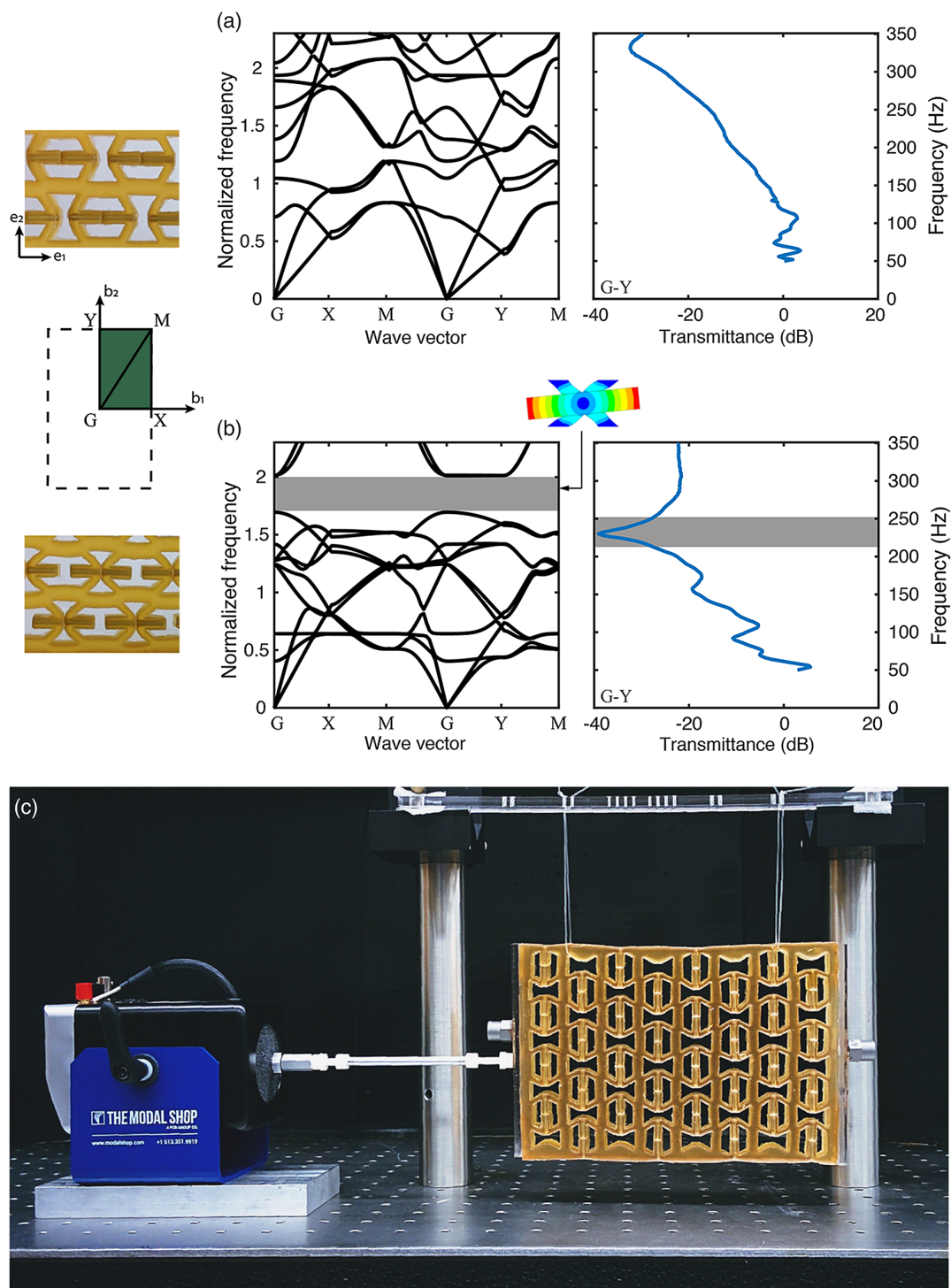


Figure 4. a) Calculated band diagrams (modal plot) for the metamaterial in the hexagonal/hourglass configuration (left), next to the transmittance curve obtained experimentally. Notice the absence of bandgaps in the frequency range shown here. b) Calculated band diagrams (modal plot) for the kagome configuration (left), next to the transmittance curve obtained experimentally. Notice the appearance of a well-defined bandgap. The resonant mode and the frequency of the “magnet beams” are depicted in the inset. c) Image of the experimental setup used to capture wave transmittance.

was 12.8 mm. The magnets were cylindrical neodymium N48 (brand emovendo), with a diameter of 3.2 mm and a length of 12.8 mm. The mold used to cast the samples was fabricated in poly(methyl

methacrylate) (PMMA) and poly(lactic acid) (PLA). The jigs used for the shear test were also manufactured in PLA. See Supporting Information for more details.

Quasistatic Experiments: All the quasistatic experiments were performed in a universal testing machine (Instron, model 8862). The tests to characterize the effective properties (Young's and shear moduli) were performed at a rate of 0.01 mm s^{-1} (strain rate of $0.04\% \text{ s}^{-1}$), with the results averaged over three nominally identical samples for each test. The rate used to characterize the cyclic behavior was 0.1 mm s^{-1} ($0.4\% \text{ s}^{-1}$). See Supporting Information for more details.

Wave Propagation Experiments: To characterize wave propagation along the e_2 direction, we fabricated a 4×4 unit cell sample, attached acrylic (PMMA) plates to both ends, and suspended the sample with nylon wires (Figure 4). Two single-axis piezoelectric accelerometers (Endevco 751-500, with a signal conditioner Endevco 2792B) were attached to the PMMA plates. Waves were introduced by an electrodynamic shaker (The Modal Shop 2007E). The data were collected using a data acquisition system (National Instruments 9215), with a sampling rate of 40 kHz.

Finite Element Analysis: The commercial finite element analysis package Abaqus 6.14 was used for the quasistatic analysis. S4 quadratic elements were used for all simulations. For the extraction of the effective properties, a steady-state, linear analysis was performed, using periodic boundary conditions. For the investigation of cyclic behavior, we used a dynamic implicit step, with nonlinear deformation enabled. The top and bottom boundaries of the model were fixed along the x direction and uniform cyclic displacements along the y direction were prescribed. The left and right boundaries were left free. The imposed duration of the analysis was 4 s, the maximum time increment was 0.05, the minimum time increment was 10^{-10} , and the maximum number of iterations was 10^6 . For the parametric study of the magnetoelastic metamaterial and the chain of arches in series, we performed nonlinear finite element analyses; for the chain of arches, 30 designs were explored within the following space: $h/L = [0.01 \text{ } 0.3]$ and $h/t = [3 \text{ } 10]$, with h , L , and t defined in Figure S11a, Supporting Information and in the literature.^[22] For the magnetoelastic metamaterial, 50 designs were explored within the following space: $t/L = [0.08 \text{ } 0.52]$; $\beta = \cos^{-1} \left[\frac{L \cos(\theta_h) + 0.5d}{L} \right] = [50^\circ \text{ } 15^\circ]$; and $F_p/(W \cdot L \cdot E_s) = [0.005 \text{ } 0.1]$, where d is the distance between magnets, F_p is the pull force of the magnets, W is the thickness of the sample, E_s is Young's modulus of the constituent material, and all other parameters are defined in Figure S5 and S11b, Supporting Information. The value of the hexagonal/hourglass angle was fixed at $\theta_h = 60^\circ$. The commercial finite element analysis package Ansys 18.2 was used to perform the wave propagation simulations. Four-node quadratic elements (Plane182) were used in all simulations, the analysis type was Modal, and the mode extraction method was Block Lanczos. The analysis was performed for 100 points in k -space. We applied Bloch-periodic boundary conditions to the edges of the unit cell.^[23–26] See Supporting Information for more details.

Supporting Information

Supporting Information is available from the Wiley Online Library or from the author.

Acknowledgements

Funding from Office of Naval Research (program manager D. Shifler, contract no. N000141110884) is gratefully acknowledged. A.G.I. thanks the Obra Social "la Caixa" and the Balsells Foundation for partial financial support. The Abaqus Finite Element Analysis software is licensed from Dassault Systemes SIMULIA, as part of a Strategic Academic Customer Program between UC Irvine and SIMULIA.

Conflict of Interest

The authors declare no conflict of interest.

Keywords

energy dissipation, kagome lattices, mechanical metamaterials, negative stiffness, wave propagation

Received: August 22, 2019

Revised: October 29, 2019

Published online:

- [1] R. Lakes, *Viscoelastic Materials*, Cambridge University Press, Cambridge **2009**.
- [2] I. Benichou, S. Givli, *J. Mech. Phys. Solids* **2013**, *61*, 94.
- [3] D. M. Correa, C. C. Seepersad, M. R. Haberman, *Integr. Mater.* **2015**, *4*, 10.
- [4] A. Rafsanjani, A. Akbarzadeh, D. Pasini, *Adv. Mater.* **2015**, *27*, 5931.
- [5] A. Guell Izard, R. Fabian Alfonso, G. McKnight, L. Valdevit, *Mater. Des.* **2017**, *135*, 37.
- [6] L. Dong, R. Lakes, *Int. J. Solids Struct.* **2013**, *50*, 2416.
- [7] B. Haghpahan, L. Salari-Sharif, P. Pourrajab, J. Hopkins, L. Valdevit, *Adv. Mater.* **2016**, *28*, 8065.
- [8] S. Shan, S. H. Kang, J. R. Raney, P. Wang, L. Fang, F. Candido, J. A. Lewis, K. Bertoldi, *Adv. Mater.* **2015**, *27*, 4296.
- [9] D. Restrepo, N. D. Mankame, P. D. Zavattieri, *Extreme Mech. Lett.* **2015**, *4*, 52.
- [10] N. Zhou, K. Liu, *J. Sound Vib.* **2010**, *329*, 1254.
- [11] R. L. Harne, K. W. Wang, *Smart Mater. Struct.* **2013**, *22*, 023001.
- [12] X. Shi, S. Zhu, *Smart Mater. Struct.* **2015**, *24*, 072002.
- [13] B. Haghpahan, H. Ebrahimi, D. Mousanezhad, J. Hopkins, A. Vaziri, *Adv. Eng. Mater.* **2016**, *18*, 643.
- [14] T. A. M. Hewage, K. L. Alderson, A. Alderson, F. Scarpa, *Adv. Mater.* **2016**, *28*, 10323.
- [15] J. Meaud, K. Che, *Int. J. Solids Struct.* **2017**, *122–123*, 69.
- [16] M. Schaeffer, M. Ruzzene, *J. Appl. Phys.* **2015**, *117*, 194903.
- [17] T. Belytschko, D. F. Schoeberle, *J. Appl. Mech.* **1975**, *42*, 865.
- [18] B. Haghpahan, A. Shirazi, L. Salari-Sharif, A. Guell Izard, L. Valdevit, *Extreme Mech. Lett.* **2017**, *17*, 56.
- [19] L. Brillouin, *Wave Propagation in Periodic Structures: Electric Filters and Crystal Lattices*, Dover Publications, New York **1953**.
- [20] F. Bloch, *Z. Physik* **1929**, *52*, 555.
- [21] Z. Liu, *Science* **2000**, *289*, 1734.
- [22] J. Qiu, J. H. Lang, A. H. Slocum, *J. Microelectromech. Syst.* **2004**, *13*, 137.
- [23] M. S. Kushwaha, P. Halevi, L. Dobrzynski, B. Djafari-Rouhani, *Phys. Rev. Lett.* **1993**, *71*, 2022.
- [24] P. Wang, J. Shim, K. Bertoldi, *Phys. Rev. B* **2013**, *88*, 014304.
- [25] M. Maldovan, E. L. Thomas, *Periodic Materials and Interference Lithography*, Wiley-VCH Verlag GmbH & Co. KGaA, Weinheim, Germany **2008**.
- [26] M. Åberg, P. Gudmundson, *J. Acoust. Soc. Am.* **1997**, *102*, 2007.